Generation of Large-Scale Magnetic Fields by Small-Scale Dynamo in Shear Flows

J. Squire and A. Bhattacharjee

Phys. Rev. Lett. **115**, 175003 — Published 20 October 2015

DOI: 10.1103/PhysRevLett.115.175003

Generation of large-scale magnetic fields by small-scale dynamo in shear flows

J. Squire* and A. Bhattacharjee
Max Planck/Princeton Center for Plasma Physics, Department of Astrophysical Sciences and Princeton Plasma Physics Laboratory, Princeton University, Princeton, NJ 08543, USA

We propose a new mechanism for turbulent mean-field dynamo in which the magnetic fluctuations resulting from a small-scale dynamo drive the generation of large-scale magnetic fields. This is in stark contrast to the common idea that small-scale magnetic fields should be harmful to large-scale dynamo action. These dynamos occur in the presence of large-scale velocity shear and do not require net helicity, resulting from off-diagonal components of the turbulent resistivity tensor as the magnetic analogue of the "shear-current" effect. Given the inevitable existence of nonhelical small-scale magnetic fields in turbulent plasmas, as well as the generic nature of velocity shear, the suggested mechanism may help explain generation of large-scale magnetic fields across a wide range of astrophysical objects.

Astrophysical magnetic fields are observed to be well-correlated over length and time scales far exceeding that of the underlying fluid motions. Beautiful in its regularity, the 22-year solar cycle is the most well-known example of this behavior [1]. Such large-scale structure is puzzling given that strong magnetic fields are expected to emerge through the stretching and twisting of field lines by smaller scale turbulence. As the primary theoretical framework to study such behavior, mean-field dynamo theory examines how large-scale magnetic fields develop due to these small-scale turbulent motions. This splitting between scales is captured by the mean-field average; the average of a fluctuating quantity vanishes by definition ($\overline{\boldsymbol{b}} = 0$), while the average of a large-scale field is itself ($\overline{\boldsymbol{B}} = \boldsymbol{B}$). An average of the induction equation, which governs evolution of the magnetic field within magnetohydrodynamics (MHD), leads to [2]

$$\partial_t \boldsymbol{B} = \nabla \times (\boldsymbol{U} \times \boldsymbol{B}) + \nabla \times \boldsymbol{\mathcal{E}} + \frac{1}{\mathrm{Rm}} \nabla^2 \boldsymbol{B}, \tag{1}$$

where Rm is the magnetic Reynolds number, a dimensionless measure of the plasma resistivity, and $\boldsymbol{U}$ and $\boldsymbol{B}$ are the large-scale velocity and magnetic field. The *electromotive force*, $\boldsymbol{\mathcal{E}} = \overline{\boldsymbol{u} \times \boldsymbol{b}}$, is an average of the fluctuating fields ($\boldsymbol{u}$ and $\boldsymbol{b}$) and responsible for dynamo action. In the early phases of a dynamo, the mean fields can be considered a small perturbation to the underlying turbulence. Combined with an assumption of scale separation between small-scale and mean fields, this allows a Taylor expansion [3, 4] of $\boldsymbol{\mathcal{E}}$ in terms of $\boldsymbol{B}$,

$$\boldsymbol{\mathcal{E}} = \alpha \circ \boldsymbol{B} + \beta \circ \nabla \boldsymbol{B} + \cdots, \tag{2}$$

where α, β are the tensorial transport coefficients, calculated from the small-scale fields [5]. Since these depend on the large-scale fields, a solution to Eq. (1) requires knowledge of how $\boldsymbol{\mathcal{E}}$ changes with $\boldsymbol{B}$ (and possibly $\boldsymbol{U}$), essentially a statistical closure for inhomogenous MHD.

Historically, much work has focused on kinematic dynamo theory, in which $\boldsymbol{u}$ is uninfluenced by the magnetic field [2, 3]. Kinematic theory predicts large-scale dynamo instability when the fluid motions possess helicity, $\int \boldsymbol{u} \cdot \nabla \times \boldsymbol{u} \, d\boldsymbol{x} \neq 0$. However, the applicability of such predictions has been called into question by a number of authors [6, 7]. In particular, above modest Reynolds numbers in both helical and nonhelical flows, the small-scale dynamo [8] causes $\boldsymbol{b}$ to grow and saturate much more rapidly [9] than $\boldsymbol{B}$. This violates the kinematic assumption, both because $\boldsymbol{u}$ is altered before $\boldsymbol{B}$ grows significantly, and because a dynamically important $\boldsymbol{b}$ exists independently of $\boldsymbol{B}$. The buildup of small-scale fields is the origin of "α quenching," in which the mean field saturates well before reaching amplitudes consistent with observation [10–13] due to the adverse influence of $\boldsymbol{b}$.

In this letter we show that in turbulence with large-scale velocity shear, it is possible and realizable to have the small-scale dynamo *enhance* the growth of the large-scale dynamo. We demonstrate this both with statistical simulation [14], in which the effect is very clear but applies rigorously only at low Reynolds numbers, and through calculation of transport coefficients from direct numerical simulations (DNS). In addition, the existence of the effect has been confirmed analytically using the second-order correlation approximation [15], which agrees with previous spectral τ approximation calculations [16].

All computations presented here use the incompressible MHD model in the shearing box, employing homogenous Cartesian geometry and periodic boundary conditions in the shearing frame. With a mean flow $\boldsymbol{U}_0 = -S\, x \hat{\boldsymbol{y}}$ imposed across the domain, this setup is designed to represent a small "patch" of turbulent fluid in large-scale velocity shear. We force with nonhelical white-in-time noise at small scales and study the generation of larger-scale magnetic fields, in a way similar to previous authors [17, 18]. The mean-field average is defined as an average over the horizontal (x and y) directions, such that the mean magnetic fields $\boldsymbol{B}$ depend only on z. We also allow for system rotation through a mean Coriolis force, since shear typically arises due to differential rotation in astrophysical objects. The rotation $\boldsymbol{\Omega}$ is aligned with $\hat{\boldsymbol{z}}$ (antiparallel to $\nabla \times \boldsymbol{U}_0$), perpendicular to the flow $\boldsymbol{U}_0$.

For the chosen horizontal average, inserting Eq. (2) into (1) gives

$$\begin{aligned} \partial_t B_x &= -\alpha_{yx} \partial_z B_x - \alpha_{yy} \partial_z B_y - \eta_{yx} \partial_z^2 B_y + \eta_{ty} \partial_z^2 B_x \\ \partial_t B_y &= -S B_x + \alpha_{xx} \partial_z B_x + \alpha_{xy} \partial_z B_y - \eta_{xy} \partial_z^2 B_x + \eta_{tx} \partial_z^2 B_y, \end{aligned} \tag{3}$$

using velocity shear $\boldsymbol{U}_0$ but neglecting other mean velocities,

and defining $\eta_{ti} \equiv \eta_{ii} + \mathrm{Rm}^{-1}$. Here α_{ij} and η_{ij} are the α effect and turbulent resistivity tensors respectively, with the 4 components of η_{ij} relatable to the β_{ij3} elements of the full tensor [Eq. (2)]. Due to homogeneity and reflectional symmetry (vanishing net helicity), α_{ij} must vanish when averaged over a suitably large time or number of realizations [3], and indeed our measurements confirm this. There is no such constraint on η_{ij}, and η_{yx} is very important throughout this work due to its coupling with the shear. In particular, neglecting fluctuations in α and assuming diagonal resistivities are equal ($\eta_{tx} = \eta_{ty} = \eta_t$), the least stable eigenmode of Eq. (3) for a mode of vertical wavenumber k grows at

$$\gamma = k\left[\eta_{yx}(-S + k^2\eta_{xy})\right]^{1/2} - k^2\eta_t. \tag{4}$$

Since $S \gg \eta_{ij}$, dynamo action is possible without an α effect if $\eta_{yx} < 0$.

Subsequent to early analytic work [19–21], it was found kinematically that $\eta_{yx} > 0$ (at least at low Rm), and several authors have thus concluded that a coherent shear dynamo cannot explain observed field generation [18, 22, 23]. Instead, a popular theory is that temporal fluctuations in α_{ij} cause an *incoherent* mean-field dynamo. Importantly, in such a dynamo, $\boldsymbol{B}(z,t)$ cannot have a constant phase in time as it grows, since the average of $\boldsymbol{B}$ over an ensemble of realizations vanishes, implying $\boldsymbol{B}$ must be uncorrelated with itself after $t \gtrsim (k^2\eta_t)^{-1}$ [24]. While incoherent dynamos are possible in a variety of situations, here we argue for a different situation – magnetic fluctuations act to substantially decrease and potentially reverse the sign of η_{yx}, causing the onset of a coherent large-scale dynamo that can overwhelm the incoherent dynamo.

Our first method illustrating this effect is quasi-linear statistical simulation; see Ref. [26] for further details. The method starts by forming equations for the fluctuating fields $\boldsymbol{u}$ and $\boldsymbol{b}$, and linearizing these; i.e., neglecting fluctuation-fluctuation nonlinearities such as $\boldsymbol{u}\cdot\nabla\boldsymbol{u}$ and $\boldsymbol{u}\cdot\nabla\boldsymbol{b}$. One can then derive an equation for the fluctuation *statistics*, $C = \langle\chi_i\chi_j\rangle$ (where $\boldsymbol{\chi} = (\boldsymbol{u},\boldsymbol{b})$ and $\langle\cdot\rangle$ denotes the average over an ensemble of realizations), as a function of $\boldsymbol{U}$ and $\boldsymbol{B}$ [14, 27, 28]. Finally, using $\mathcal{E}_x = \overline{C_{26} - C_{53}}$ and $\mathcal{E}_y = \overline{C_{34} - C_{61}}$, $\boldsymbol{\mathcal{E}}$ can be fed directly into Eq. (1), resulting in a closed system of equations. Note that the method does not assume a scale separation between mean and fluctuating fields. Importantly, since the statistics are calculated directly, an incoherent dynamo is not possible, and statistical simulation offers a direct probe of the coherent effect. The linearity of the fluctuation equations eliminates the small-scale dynamo; accordingly, to excite homogenous kinetic and magnetic fluctuations, both $\boldsymbol{u}$ and $\boldsymbol{b}$ are forced at small scales ($k_f = 6\pi$) with the statistics of white-in-time noise. The resulting MHD turbulent bath could be considered as some approximation to kinetically forced turbulence after saturation of the small-scale dynamo.

To study the magnetically driven dynamo, we keep the total forcing level constant, successively increasing the proportion of magnetic forcing from purely kinetic [25]. Results with shear but no rotation are illustrated in Fig. 1. The presence of the magnetically driven dynamo is evident, becoming slightly unstable when magnetic forcing accounts for 0.4 of the total and increasing the growth rate thereafter. This sustained period of exponential growth due to magnetic fluctuations is not possible to see in DNS, since the mean field will immediately come into approximate equipartition with the small-scale field due to the finite size of the system.

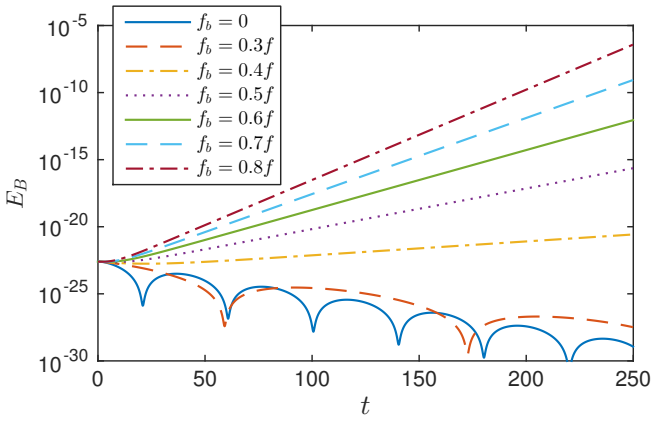

FIG. 1. Time development of the mean-field energy, $E_B = \int dz\, B^2/2$, in quasi-linear statistical simulation. Small-scale fields are forced at $k_f = 6\pi$, $\mathrm{Rm} = u_{rms}/\eta k_f \approx 5$ (here η is the resistivity, $\mathrm{Pm} = \mathrm{Rm}/\mathrm{Re} = 1$), $S = 2$ and the box has dimensions $\left(L_x, L_y, L_z\right) = (1, 1, 4)$ with resolution $(28, 28, 128)$. As well as forcing the momentum equation, the induction equation is forced to excite homogenous magnetic fluctuations, emulating a small-scale dynamo. Total forcing is kept constant in each simulation but the proportion of magnetic forcing (f_b/f) is increased from 0 to 0.8 [25]. As f_b/f increases, the growth rate of the mean field increases due to the change in sign and subsequent decrease of η_{yx}.

The formal applicability of statistical simulation is limited to low Rm due to the quasi-linear approximation. Our second method utilizes DNS, forced kinetically at small scales, to show that magnetic fields arising consistently *through the small-scale dynamo* can drive a coherent large-scale dynamo. To this end, we directly calculate transport coefficients from nonlinear simulation before and after the saturation of the small-scale dynamo. We use the incompressible MHD code SNOOPY [29], which uses the pseudo-spectral method and shearing-periodic boundary conditions. In line with our goal of showing that the effect is possible, we choose moderate Reynolds numbers [17], running ensembles of 100 simulations with shear $\boldsymbol{U}_0 = -S\,x\hat{\boldsymbol{y}}$, both with and without Keplerian rotation. The moderate Reynolds numbers have the benefit of ensuring there is no self-sustaining turbulence in the absence of small-scale forcing (although effects may be similar even when this occurs [30]), as well as reducing the numerical burden of each simulation, which enables many simulations to be run with different noise realizations (around 400 CPU hours are required to compute each realization). At these parameters, the prevalence of the coherent large-scale dynamo depends on the realization (see Fig. 2), and it appears that the coherent effect cannot always overcome fluctuations in $\boldsymbol{\mathcal{E}}$ im-

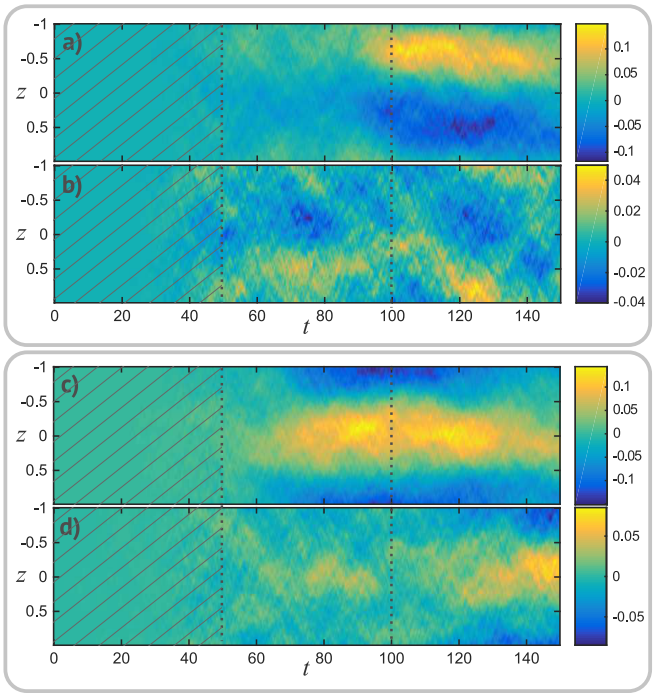

FIG. 2. Example spatiotemporal B_y evolutions for non-rotating (a-b) and Keplerian rotating (c-d) turbulence at Rm $= u_{rms}/\eta k_f \approx 15$ ($k_f = 6\pi$, $\eta = 1/2000$, Pm $= 8$), $S = 1$, in a box of dimension $(1, 4, 2)$ with resolution $(64, 128, 128)$. The first examples in each case [(a) and (c)] show B_y when a coherent dynamo develops, while the second examples [(b) and (d)] illustrate the case when it is more incoherent. The main factors in distinguishing these are the coherency in phase of B_y over some time period and the amplitude at saturation, which is larger in the coherent cases. In general, the rotating simulations are substantially more coherent. The hatched area illustrates the region of small-scale dynamo growth. The fitting method used to compute transport coefficients (see Fig. 3) is applied between the dashed lines ($t = 50 \rightarrow 100$).

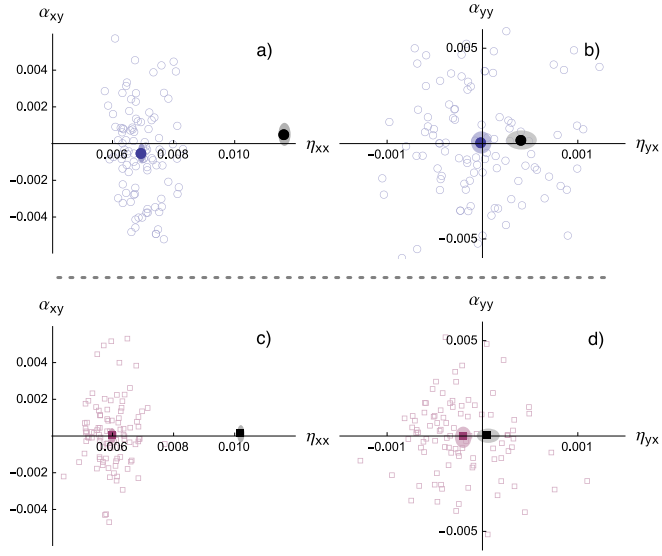

FIG. 3. Measurements of the turbulent transport coefficients for 100 realizations of the simulations at the same parameters as those in Fig. 2; (a) η_{xx} and α_{xy} coefficients (x and y axes respectively), no rotation, (b) η_{yx} and α_{yy} coefficients, no rotation, (c) η_{xx} and α_{xy} coefficients, rotating, (b) η_{yx} and α_{yy} coefficients, rotating [see Eq. (3)]. Unfilled markers in each plot show coefficients measured from each of the individual realizations, with mean values displayed with solid markers and the shaded regions indicating error in the mean (2 standard deviations). Black markers illustrate the kinematic transport coefficients, with grey shaded regions indicating the error. After saturation of the small-scale dynamo, we calculate $\alpha_{ij}(t)$ and $\eta_{ij}(t)$ by solving Eq. (2) approximately (see text), taking the mean from $t = 50$ to $t = 100$. This limited time window is chosen to avoid capturing the saturation phase of the large-scale dynamo, since η_{ij} is presumably modified in this phase. In both methods of computing transport coefficients, α coefficients are zero to within error as expected, and the scatter between simulations is of a similar magnitude to that of η_{ij} if one accounts for their different units (it is necessary to divide α by a characteristic k value).

mediately after small-scale saturation, although the dynamo develops after a sufficiently long time [e.g., Fig. 2(d) near $t = 150$]. This behavior seems generic when the coherent dynamo is close to its threshold for excitation and we have observed similar structures when the induction equation is driven directly at lower Rm [26]. Notwithstanding this variability in the dynamo's qualitative behavior, measurement of the transport coefficients illustrates that the η_{yx} coefficient decreases after the magnetic fluctuations reach approximate equipartition with velocity fluctuations at small scales.

At low times, we use the test-field method to measure the kinematic α and η, fixing the mean field and calculating $\boldsymbol{\mathcal{E}}$, with no Lorentz force [3, 18]. Since the small-scale dynamo grows quickly, test-fields are reset every $t = 5$. After small-scale saturation, standard test-field methods are inapplicable [31]. Instead, we extract $\boldsymbol{B}$ and $\boldsymbol{\mathcal{E}}$ simulation data and calculate $(\alpha_{ij}(t), \eta_{ij}(t))$ directly from Eq. (2) by computing $\int dz\, \mathcal{E}_i \Theta$ for each of $\Theta = (B_x, B_y, \partial_z B_x, \partial_z B_y)$ and solving the resulting matrix equations (in the least-squares sense) at each time point. This method is similar to that presented in Ref. [32]; however, we additionally impose the constraints $\eta_{yy}(t) = \eta_{xx}(t)$, $\alpha_{xx}(t) = \alpha_{yy}(t)$ and $\alpha_{yx}(t) = \eta_{xy}(t) = 0$. While these changes may appear to make the method less accurate, they in fact achieve the opposite by reducing the influence of B_x. This is necessary because B_x has a high level of noise in comparison to its magnitude, and because this noise is correlated with the noise in B_y (due to B_x directly driving B_y) and $\mathcal{E}_y$ (through $\partial_t B_x = -\partial_z \mathcal{E}_y + \cdots$). These correlations are very harmful to the quality of the fit, causing unphysical negative values for η_{yy} [32], which also pollute measurement of other coefficients. It is straightforward to show that the systematic errors caused by our constraints on the transport coefficients are less than 1% for the dynamos in Fig. 2, so long as $\eta_{xx} \approx \eta_{yy}$ when time averaged. We have verified the method is accurate by comparison with the kinematic test-field method at low Rm, where there is no small-scale dynamo [26, 33] and the rotation can be used to explore a range of η_{yx}. In addition, the measurements are independently verified in Fig. 4 below [34]. Due to the short time-window, measurements

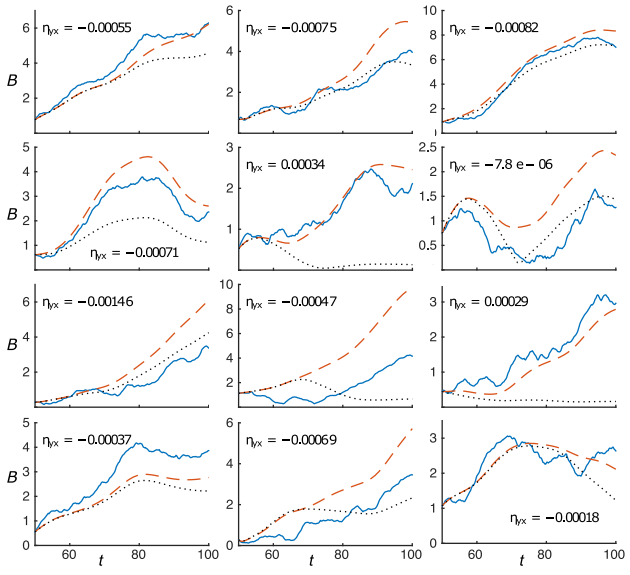

FIG. 4. Evolution of the mean-field magnitude for a sample of the ensemble of rotating simulations (Figs. 2–3). Here B, the mean-field magnitude, is $(|\hat{B}_x^1|^2 + |\hat{B}_y^1|^2)^{1/2}$ where $\hat{B}_i^1$ is the largest scale Fourier mode of B_i. In each plot the solid blue curve shows data taken from the simulation. The dashed red curve shows the corresponding expected evolution, using the time-dependent calculated values of the transport coefficients, smoothed in time using a Gaussian filter of width 5. Finally, the dotted black curve illustrates the expected evolution with all α coefficients artificially set to zero. The similarity between this evolution and that including α (dashed curve) illustrates that in many (but not all) cases the dynamo is primary driven by η_{yx}. We list the measured mean of η_{yx} in each plot to show that lower values generally lead to stronger mean-field growth, as expected for a coherent dynamo. For reference, at the measured $\eta_{xx} \approx 0.006$, the coherent dynamo is unstable below $\eta_{yx} = -0.00036$.

of the transport coefficients after small-scale saturation vary significantly between realization, as should be expected from Fig. 2. Nonetheless, an average over the ensemble of 100 simulations illustrates a statistically significant change in η_{yx} that is consistent with observed behavior.

Results are illustrated in Fig. 3. In the kinematic phase without rotation, we see $\eta_{yx} = (4.1 \pm 1.6) \times 10^{-4}$ in qualitative agreement with previous studies [18]. With rotation $\eta_{yx} = (0.6 \pm 1.2) \times 10^{-4}$, consistent with a reduction in η_{yx} due to the $\boldsymbol{\Omega} \times \boldsymbol{J}$ effect [5]. After saturation of the small-scale dynamo, $\eta_{yx} = (-0.1 \pm 1.0) \times 10^{-4}$ for the non-rotating case, while $\eta_{yx} \approx -(2.0 \pm 0.8) \times 10^{-4}$ in the rotating case – the same reduction in each to within error. Values for the diagonal resistivity are smaller after saturation, as expected since the velocity fluctuation energy decreases (by a factor ~ 1.4). The values of (η_{xx}, η_{yx}) show that the dynamo is slightly stable on average in the non-rotating case and marginal in the rotating case. However, the coefficients vary significantly between realizations, sometimes yielding larger growth rates, and measurements match observed growth of the mean field for individual realizations. We illustrate this in Fig. 4, which demonstrates consistency between the measured transport coefficients and observed mean-field evolution by solving Eq. (3) directly [using the time-dependent η_{ij}(t) and $\alpha_{ij}(t)$], for a sample of the rotating simulations. In addition, by artificially removing $\alpha_{ij}(t)$, we illustrate that cases with more negative η_{yx} are driven primarily by this, rather than a stochastic-α effect. We thus conclude that small-scale magnetic fluctuations act to *decrease* η_{yx}, and that in some realizations (or after a sufficiently long time period) a coherent large-scale dynamo develops as a result.

To summarize, in this letter we have demonstrated that small-scale magnetic fluctuations, excited by small-scale dynamo action, can drive large-scale magnetic field generation. The mechanism is a magnetic analogue of the "shear-current" effect [16, 21], arising through the off-diagonal turbulent resistivity in the presence of large-scale shear flow. We have demonstrated its existence numerically using both DNS, with measurements of mean-field transport coefficients before and after small-scale dynamo saturation, and through quasi-linear statistical simulation.

More work is needed to precisely assess regimes in which the magnetically driven dynamo might dominate, as well as its behavior at higher Reynolds numbers where self-sustained turbulence is possible [30]. Another interesting question regards whether a magnetic dynamo can remain influential in the presence of net helicity and an α effect, particularly as small-scale dynamo may be suppressed by shear [35]. While such questions may be difficult to answer definitively, the generic presence of magnetic fluctuations in plasma turbulence gives us some confidence that the proposed mechanism could cause large-scale dynamo growth in the wide variety of astrophysical systems with velocity shear.

This work was supported by a Procter Fellowship at Princeton University, and the US Department of Energy Grant DE-AC02-09-CH11466. The authors would like to thank A. Schekochihin, J. Krommes, and I. Rogachevskii for enlightening discussion and useful suggestions, as well as G. Lesur for making the SNOOPY code freely available.

* jsquire@princeton.edu

[1] D. H. Hathaway, Living Reviews in Solar Physics **7**, 1 (2010).
[2] H. K. Moffatt, *Magnetic Field Generation in Electrically Conducting Fluids* (Cambridge University Press, 1978).
[3] A. Brandenburg and K. Subramanian, Phys. Rep. **417**, 1 (2005).
[4] N. Yokoi, Geophys. Astrophys. Fluid Dyn. **107**, 114 (2013).
[5] F. Krause and K. H. Rädler, *Mean-field magnetohydrodynamics and dynamo theory* (Oxford: Pergamon Press, 1980).
[6] R. M. Kulsrud and S. W. Anderson, Astrophys. J. **396**, 606 (1992).
[7] F. Cattaneo and D. W. Hughes, Mon. Not. R. Astron. Soc. **395**, L48 (2009).
[8] A. A. Schekochihin *et al.*, New J. Phys. **9**, 300 (2007).
[9] S. Boldyrev, F. Cattaneo, and R. Rosner, Phys. Rev. Lett. **95**, 255001 (2005).
[10] A. V. Gruzinov and P. H. Diamond, Phys. Rev. Lett. **72**, 1651 (1994).

[11] A. Bhattacharjee and Y. Yuan, Astrophys. J. **449**, 739 (1995).
[12] E. G. Blackman and G. B Field, Phys. Rev. Lett. **89**, 265007 (2002).
[13] H. Hotta, M. Rempel, and T. Yokoyama, Astrophys. J. **803**, 42 (2015).
[14] J. Squire and A. Bhattacharjee, Phys. Rev. Lett. **114**, 085002 (2015).
[15] J. Squire and A. Bhattacharjee, (2015), *in preparation*.
[16] I. Rogachevskii and N. Kleeorin, Phys. Rev. E **70**, 046310 (2004).
[17] T. A. Yousef *et al.*, Astron. Nachr. **329**, 737 (2008).
[18] A. Brandenburg, K. H. Rädler, M. Rheinhardt, and P. J. Käpylä, Astrophys. J. **676**, 740 (2008).
[19] V. Urpin, Astron. Astrophys. **347**, L47 (1999).
[20] V. Urpin, Phys. Rev. E **65**, 026301 (2002).
[21] I. Rogachevskii and N. Kleeorin, Phys. Rev. E **68**, 036301 (2003).
[22] K.-H. Rädler and R. Stepanov, Phys. Rev. E **73**, 056311 (2006).
[23] N. K. Singh and S. Sridhar, Phys. Rev. E **83**, 056309 (2011).
[24] This condition may be altered if one considers the effects of magnetic helicity conservation, which may cause a local magnetic α effect as the large-scale field grows [18]. However, this also causes coupling between different mean-field modes, and the detailed consequences of such an effect remain unclear.
[25] Specifically, for the forcing $\boldsymbol{f}_i$ (acting through $\partial_t \boldsymbol{u} = \cdots + \boldsymbol{f}_u$ and $\partial_t \boldsymbol{b} = \cdots + \boldsymbol{f}_b$), we keep $\boldsymbol{f} = \boldsymbol{f}_u + \boldsymbol{f}_b$ constant (in the statistical sense) across all simulations in Fig. 1.
[26] J. Squire and A. Bhattacharjee, ArXiv e-prints (2015), arXiv:1507.03154 [astro-ph.HE].
[27] B. F. Farrell and P. J. Ioannou, J. Fluid Mech. **708**, 149 (2012).
[28] S. M. Tobias, K. Dagon, and J. B. Marston, Astrophys. J. **727**, 127 (2011).
[29] G. Lesur and P. Y. Longaretti, Mon. Not. R. Astron. Soc. **378**, 1471 (2007).
[30] G. Lesur and G. I. Ogilvie, Astron. Astrophys. **488**, 451 (2008).
[31] M. Rheinhardt and A. Brandenburg, Astron. Astrophys. **520**, A28 (2010).
[32] A. Brandenburg and D. Sokoloff, Geophys. Astrophys. Fluid Dyn. **96**, 319 (2002).
[33] T. A. Yousef *et al.*, Phys. Rev. Lett. **100**, 184501 (2008).
[34] Ideally, one would utilize the same method to measure transport coefficients before and after small-scale saturation. However, the very fast growth of the small-scale field at early times renders the passive transport coefficient measurement unfeasible, since the mean field is dominated by small-scale fields and Eq. (2) does not apply.
[35] S. M. Tobias and F. Cattaneo, Nature **497**, 463 (2014).